Fluorochrome-Functionalized Nanoparticles for Imaging DNA in Biological Systems

Hoonsung Cho,[†] David Alcantara,[‡] Hushan Yuan,[†] Rahul A. Sheth,[§] Howard H. Chen,[⊥] Peng Huang,[∥] Sean B. Andersson,[∥,¶] David E. Sosnovik,[⊥] Umar Mahmood,[†,§] and Lee Josephson[†,⊥,*]

[†]Center for Translational Nuclear Medicine and Molecular Imaging, [§]Division of Nuclear Medicine & Molecular Imaging, Department of Radiology, and [⊥]Martinos Center for Biomedical Imaging, Massachusetts General Hospital, Charlestown, Massachusetts 02129, United States, [‡]Instituto de Nanociencia de Aragon, Universidad de Zaragoza, Spain, and [∥]Department of Mechanical Engineering and [¶]Division of Systems Engineering, Boston University, Massachusetts 02215, United States

ABSTRACT Attaching DNA binding fluorochromes to nanoparticles (NPs) provides a way of obtaining NPs that bind to DNA through fluorochrome mediated interactions. To obtain a nanoparticle (NP) that bound to the DNA in biological systems, we attached the DNA binding fluorochrome, TO-PRO 1 (TO), to the surface of the Feraheme (FH) NP, to obtain a fluorochrome-functionalized NP denoted TO-FH. When reacted with DNA *in vitro*, TO-FH formed microaggregates that were characterized by fluorescence, light scattering, and T2 changes. The formation of DNA/TO-FH microaggregates was also characterized by AFM, with microaggregates exhibiting a median size of 200 nm, and consisting of DNA and multiple TO-FH NPs whose individual diameters were only 25−35 nm. TO-FH failed to bind normal cells in culture, but treatment with chemotherapeutic agents or detergents yielded necrotic cells that bound TO-FH and vital fluorochromes similarly. The uptake of TO-FH by HT-29 xenografts (treated with 5-FU and oxaliplatin) was evident by surface fluorescence and MRI. Attaching multiple DNA binding fluorochromes to magnetic nanoparticles provides a way of generating DNA binding NPs that can be used to detect DNA detection by microaggregate formation *in vitro*, for imaging the DNA of necrotic cells in culture, and for imaging the DNA of a tumor treated with a chemotherapeutic agent. Fluorochrome functionalized NPs are a multimodal (magnetic and fluorescent), highly multivalent ($n \approx 10$ fluorochromes/NP) nanomaterials useful for imaging the DNA of biological systems.

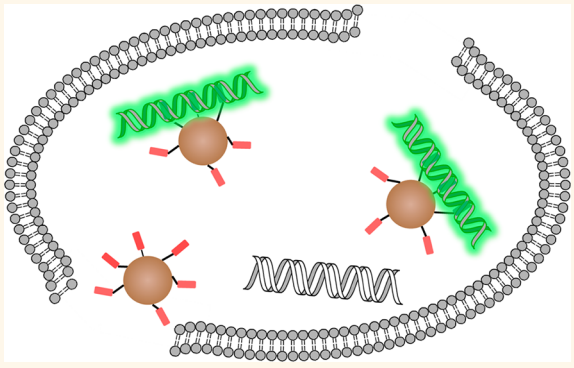

KEYWORDS: DNA · imaging · nanoparticle · fluorochrome · biosensing

The recognition of DNA by surfaces used for its purification, extraction, and manipulation often exploits one of two general types of recognition. Many DNA binding surfaces utilize electrostatic interactions between a surface charge and DNA's many negatively charged phosphates,[1,2] while others exploit sequence specific hybridization reactions between solution DNA and a solid phase, synthetic oligonucleotide.[3−6] On the other hand, the detection of DNA molecules in gels, in cells (*e.g.*, FACS), and in solution (*e.g.*, RT-PCR) often exploits the ability of molecules to fluoresce upon intercalation with DNA. Here we continue to explore how TO-PRO 1, which binds DNA through intercalation,[7,8] and which has been used as a vital fluorochrome for necrotic cells,[9−11] can be attached to magnetic NP surfaces, generating a third, and potentially general, principle of fluorochrome-mediated DNA recognition by surfaces.[12]

A key variable in the design of fluorochrome-functionalized NPs, one not found with low molecular weight DNA binding fluorochromes, is the number (density) of fluorochromes on the NP surface. Surface functionalization of NPs can generate materials with numbers of fluorochromes per NP (n) exceeding the two of fluorochrome dimers.[8,13−15]

The current study had three principal goals: (i) to obtain fluorochrome-functionalized NPs with controlled but variable numbers of intercalating fluorochromes (n) per NP, (ii) using NPs from goal (i), characterize the physical properties and reaction with DNA *in vitro* and, (iii) to select a level fluorochrome

* Address correspondence to ljosephson@mgh.harvard.edu.

Received for review September 12, 2012 and accepted February 1, 2013.

Published online February 01, 2013
10.1021/nn305962n

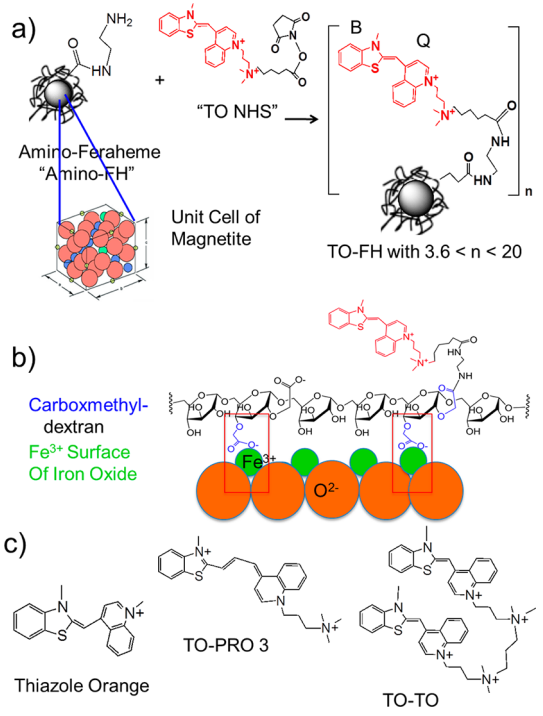

Figure 1. Synthesis and properties of fluorochrome-functionalized NPs. (a) Reacting the "TO NHS ester" with the amino-Feraheme generated fluorochrome-functionalized NPs bearing different numbers of fluorochromes (*n*) per NP. The benzothiazole (B) and quinoline (Q) rings of TO-PRO1 are shared by the low molecular reference fluorochromes: thiazole orange, TO-PRO 3, and TO-TO whose structures are given in Figure 1c. (b) Surface chemistry for fluorochrome-functionalized NPs. The carboxymethyldextran provides carboxyl groups for fluorochrome attachment and bind to the iron oxide, generating high thermal stability. (c) Structures of reference fluorochromes containing the benzothiazole (B) and quinoline (Q) rings of TO-PRO 1. Structure of TO-PRO 1 is in red in panel A.

functionalization and demonstrate the reaction of that NP with the DNA of biological systems. We show for the first time that fluorochrome-functionalized NPs, materials far bigger and far more polyvalent than previous fluorochromes, are capable of binding the DNA of necrotic cells and a tumor xenograft treated with chemotherapeutic agents. Fluorochrome-functionalized NPs are multimodal (magnetic and fluorescent), high multivalency nanomaterials useful for imaging the DNA of biological systems.

RESULTS

We attached varying numbers of the TO-PRO 1 fluorochrome per NP to an aminated version of the Feraheme (FH) nanoparticle as shown in Figure 1a. Amino-FH was then reacted with "TO-NHS," an *N*-hydroxysuccinimide ester of TO-PRO 1, to generate fluorochrome-functionalized NPs. (Feraheme is a trademark of AMAG Pharmaceuticals.)

FH is NP with an iron oxide core (5784 Fe/core, diameter of 6.4 ± 0.4 nm) and a thick coating of carboxymethyldextran. FH has a distribution of sizes

TABLE 1. Physical Properties of Feraheme (FH) and Fluorochrome-Functionalized NPs

no. of fluorochromes (*n*)	diameter (nm)	zp (mV)	r_2 ($mM^{-1}\cdot sec^{-1}$)
0 (FH)	18.2	−37.2	62.7
3.6	18.2	−14.5	55.0
4.0	29.0	−27.0	71.0
5.5	32.2	−14.7	55.6
5.8	28.0	−32.0	58.0
6.0	27.0	−12.0	78.0
7.8	25.0	−18.3	85.0
8.2	32.1	−17.5	81.0
17.0	53.0	−12.0	82.0
19.0	48.0	−9.0	72.0
20.0	42.0	−11.0	89.0

by gel permeation chromatography, with peak globular equivalent protein volume of 731 kDa.[16] By our light scattering method, FH had a hydrodynamic volume of 18.2 nm (Table 1), while the manufacturer's package insert gives a size range of 17−31 nm. Therefore most of FH's volume reflects its carboxymethyl dextran coating.[17,18] FH does not have a single molecular weight, but its size distribution is sufficiently narrow to provide reproducible safety and efficacy from lot to lot, and therefore to permit its approval in the US and EC for the treatment of iron anemia.

A model of the surface chemistry of fluorochrome-functionalized NPs is shown in Figure 1b, in which the carboxymethyl (CM) groups of the carboxymethyl dextran coating of FH provide sites for conjugation chemistry and afford high stability between the CM-dextran and iron oxide core. Screening studies of the temperature stability of polymeric coated iron oxides have shown that CM-dextran, unlike dextran coatings, produce NPs that are extremely stable to heat stress.[19] For Feraheme (FH) a high thermal stability is evident from the heat stress used for its terminal sterilization,[18] and by its storage as a room temperature liquid. TO-PRO 1, like the related fluorochromes thiazole orange and TO-TO (Figure 1c), binds DNA through the intercalation of pairs of benzothiazole (B) and quinoline (Q) rings, which generates fluorescence.[7,8,20]

To select a level of fluorochrome functionalization for imaging the DNA in biological systems with a NP, amino-Feraheme was reacted with varying amounts TO-NHS, to yield a panel of fluorochrome-functionalized NPs with different numbers of fluorochromes per NP (different values of *n*) shown in Table 1. TO-NHS (or its acid) adhered tenaciously to Sephadex G-25 (Supporting Information, Figure S1) and permitted an accurate calculation of *n*, an average ratio of fluorochromes per NP, with a value of 5784 Fe's per NP provided by the manufacturer. The molecular weights of individual TO-FH species cannot be analyzed by mass spectroscopy, as has been done in other systems,[21,22] because the molecular weight of the functional ligand (TO-PRO 1) is small compared to the

TABLE 2. Reaction of Fluorochrome Functionalized NPs with DNA by Fluorescence (Δfluor.), T_2 changes (ΔT_2), and light scattering (Δsize)

compound	figure	*n*	NP, nM	conc. fluor. equiv[a], nM	max Δfluor., au	conc. DNA @ EC50, μg/mL
Thiaz. Or.	2b	1	NA	50.0	979	1.52
TO-PRO3	2b	1	NA	50.0	2750	2.27
TO-TO	2b	2	NA	50.0	3240	0.17
TO-PRO1	2b	1	NA	50.0	1920	0.23
TO-FH	2b	3.6	13.9	50.0	2090	0.22
TO-FH	2b	8.2	6.10	50.0	2710	0.23
TO-FH	2b	17	2.94	50.0	4400	0.36
TO-FH	2b	20	2.50	50.0	5770	0.47

compound	figure	*n*	NPs, nM	conc. fluor. equiv, nM	max Δfluor., au	conc. DNA @ EC50, μg/mL
TO-FH	3c	3.6	15.2	54.7	1996.4	0.382
TO-FH	3c	8.2	15.2	124.6	5731.6	0.736
TO-FH	3c	17	15.2	258.4	9430	1.105

compound	figure	*n*	Conc NPs, nM	conc. fluor. equiv, nM	max ΔT_2, msec	conc. DNA @ EC50, μg/mL
TO-FH	3c	3.6	15.2	54.7	409.3	0.018
TO-FH	3c	8.2	15.2	124.6	535.9	0.055
TO-FH	3c	17	15.2	258.4	590.1	0.071

compound	figure	*n*	Conc NPs, nM	conc. fluor. equiv, nM	max Δsize nm	conc. DNA @ EC50, μg/mL
TO-FH	3c	3.6	15.2	54.7	166.6	0.013
TO-FH	3c	8.2	15.2	124.6	166	0.027
TO-FH	3c	17	15.2	258.4	179	0.032

[a] Fluorochrome concentrations are expressed molar equivalents of the common benzothiazole ring. NA = not applicable.

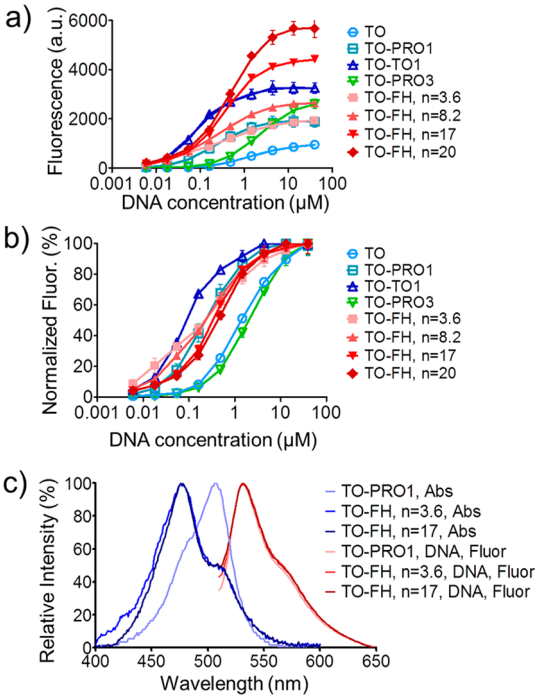

Figure 2. Reaction between fluorochrome-functionalized NPs, with different numbers of TO-PRO 1 per NP (*n*), and DNA as obtained by fluorescence. Data were obtained at 50 nM in benzothiazole equivalents with variable NP concentrations. Fluorescence responses from panel a were fit to the logit equation as shown in panel b, with the EC50 and maximum fluorescence values (max. fluor) given in Table 2. Thiazole orange and TO-PRO 3 had higher EC50 values, while fluorochrome-functionalized NPs had similar EC50 values. (c) Absorption and emission spectra of TO-FH NPs (*n* = 3.6 or 17) and TO-PRO 1. TO-FH spectra differ from TO-PRO 1 spectra due to fluorochrome/fluorochrome stacking interactions on the NP surface.

variation of the starting FH. The polydispersity of FH reflects, at least in part, the use of carboxymethyldextran polymers for a coating that are not monodisperse.[18]

Modification of the carboxyl groups leads to an increase in hydrodynamic volume by light scattering (Table 1), which measures how extended the carboxymethyldextran coating has become. An increase in size and an increased r_2 are interrelated and positively correlated in many studies with magnetic NPs.[23] NP sizes (diameters by light scattering), relaxivities (r_2 values), and zeta potentials of the fluorochrome-functionalized NP panel are given in Table 1, with *n* values ranging from as low as 3.6 to as high as 17.0 (Table 2). Size determined by light scattering is a measurement of hydrodynamic volume rather than molecular weight.

The zeta potential of FH was strongly negative (−37.2 mV) and remained negative with the attachment of amine groups and TO-PRO 1. All NPs were highly stable during storage in PBS at four degrees centigrade. Fluorochrome-functionalized NPs with varying *n* values were then examined for their interaction with DNA by fluorescence (Figure 2), by changes in T_2 relaxation times (Figure 3), and by light scattering (Figure 3).

The reaction of fluorochrome-functionalized NPs (Table 1) with DNA by fluorescence is shown in Figure 2. Also shown is the response obtained with two low molecular weight fluorochromes containing the same benzothiazole and quinolone rings as the TO-PRO 1 used in TO-FH synthesis; these were thiazole orange and TO-PRO 3 whose structures are given in Figure 1c. Using the logit equation, EC50 and maximal fluorescence (max. fluor.) values were obtained (Figure 2b) and are listed in Table 2. The absorption and emission spectra of TO-FHs and TO-PRO 1 are shown in Figure 2c; TO-FHs had distinctly different absorption spectra from TO-PRO 1 indicating a high degree of interactions and stacking among TO-PRO 1 surface fluorochromes.[24]

The interactions of fluorochrome-functionalized NPs (Table 1) with DNA by two techniques sensitive to the formation of NP/DNA microaggregates are shown in Figure 3; these were changes in the spin−spin relaxation time, ΔT_2 (Figure 3a), and changes in microaggregate size by laser dynamic light scattering (DLS), Δsize (Figure 3b). Data were fit to the logit equation (Figure 3c), yielding EC50s, values for the maximal

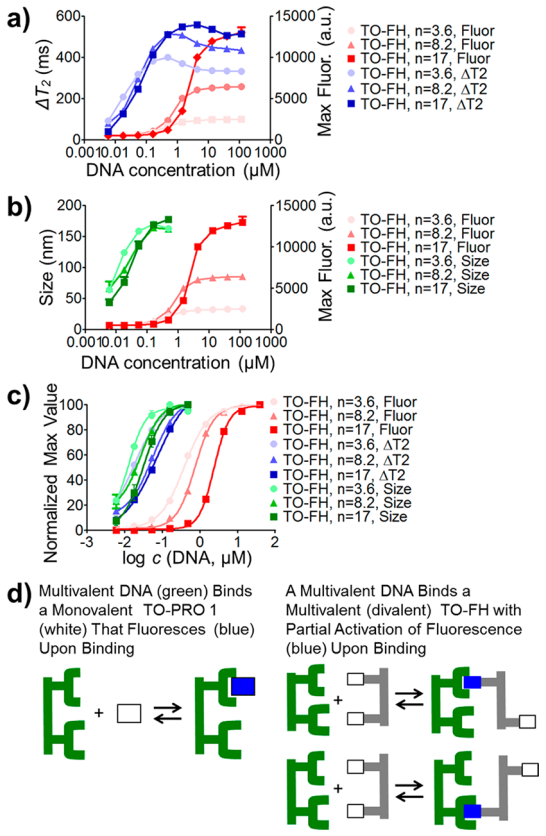

Figure 3. Reaction between TO-FHs with DNA by techniques that measure NP/DNA microaggregate formation. Microaggregate response (at a constant NP concentration of 15.2 nM) was measured by T_2 changes (a) or by light scattering (b). Fluorescence response, which differed from that of Figure 2 because of the use of fixed NP concentrations, is also shown in panels a and b. Data were analyzed by the logit equation (c) with values provided in Table 2. (d) Monovalent and divalent binding modes: the monomeric TO-PRO 1 produces its full fluorescence (blue) upon binding to DNA. A multivalent, fluorochrome-functionalized NP, represented as simplified divalent fluorochrome, has binding modes that are inefficient with respect to fluorochrome activation which occurs on DNA binding (blue).

changes in T_2 (max. ΔT_2) and values for maximal changes in microaggregate size (max. Δsize) again provided in Table 2. As shown in Table 2, EC50s for the reaction between fluorochrome-functionalized NPs and DNA were about 20-fold lower when measured by techniques sensitive to NP/DNA microaggregate formation (T_2, light scattering), when compared to the EC50s obtained by fluorescence.

A model explaining this difference in EC50s is shown in Figure 3d, where the binding of a multivalent NP and multivalent DNA is shown. The NP and DNA are considered to be divalent, the simplest case of multivalency. With monomeric TO-PRO 1 fluorescence and binding are similar events and yield similar EC50s. With multivalent TO-FH NPs, DNA/NP microaggregates form with some fluorochromes are not binding to DNA or fluorescing. At the EC50s associated with microaggregate formation (T_2 or light scattering) many fluorochromes on TO-FH cannot participate in DNA binding

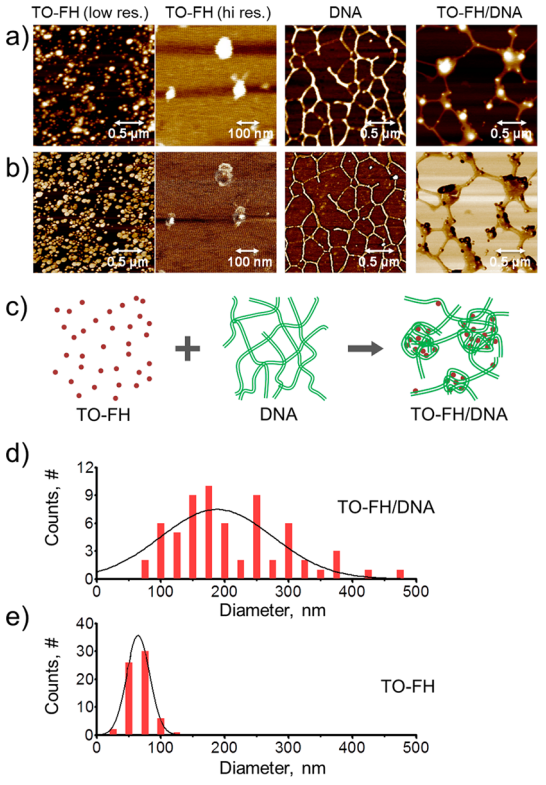

Figure 4. AFM images of DNA/TO-FH microaggregates and TO-FH. Topographic (a) and phase images (b) of DNA/TO-FH microaggregates, DNA, and TO-FH. (c) Schematic of the binding to TO-FH to DNA; (d) size distribution of DNA/TO-FH microaggregates; (e) size distribution of TO-FH. Lines are Gaussian distributions.

because there are simply not sufficient intercalation sites on DNA available. (See discussion and Supporting Information, Table S1 for the comparison fluorochrome concentrations and the concentrations of sites available for fluorochrome intercalation on DNA.)

To ensure our TO-FH preparations were uniform with respect to DNA interactions, we studied the functional interactions between TO-FH and DNA for NPs with n values ranging from as low as 3.6 to as high as 17.0 (Table 2). A narrow range of TO-FHs were selected ($7 < n < 11$) for studies using TO-FH in biological systems, since NPs in this range had high max fluor. and low EC50 values for microaggregate formation (Table 2).

To further confirm that the T_2 and light scattering changes seen in Figure 3 reflected DNA/TO-FH microaggregates, topographic and phase atomic force microscopy (AFM) images were obtained after TO-FH was incubated with DNA (Figure 4). As expected DNA appeared as polymeric threads on topographic (Figure 4a) and phase images (Figure 4b), while TO-FH NPs had diameters between 50 and 100 (Figure 4a,b,e). A schematic depiction of these results is presented in Figure 4c. AFM of DNA/TO-FH mixtures showed globular microaggregates ranging in size from 50 nm to about 400 nm (Figure 4d) and connected by DNA, consistent with microaggregate sizes seen with light

scattering (Figure 3b), and indicating that many microaggregates consist of more than one TO-FH NP. Size distributions of DNA/TO-FH microaggregates and the starting TO-FH NP from AFM studies are provided in Figure 4 panels d and e, respectively.

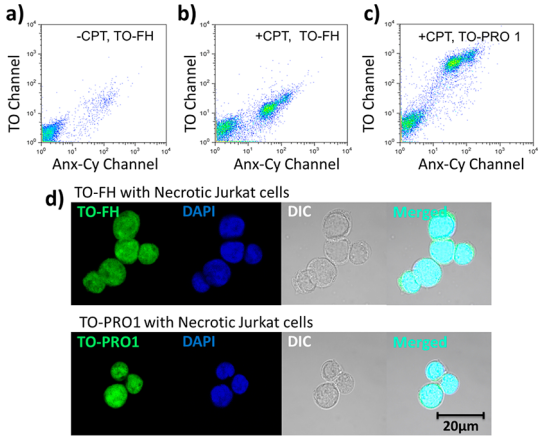

Figure 5. Interaction of TO-FH or TO-PRO 1 with the DNA of Jurkat T cells. Cells were induced into necrosis by camptothecin (CPT). (a) Dual wavelength scatter plots for control cells (−CPT) reacted with an annexin V-Cy5.5 (Anx-Cy) and TO-FH are shown. With −CPT, a small Anx-Cy, TO-FH positive population is obtained. Scatter plots for CPT-treated cells reacted with Anx-Cy and TO-FH (b) or reacted with Anx-Cy and TO-PRO 1 (c) are shown. CPT increased the population of necrotic cells that bound both TO-FH and Anx-Cy or both TO-PRO 1 and Anx-Cy. (d) Confocal microscopy of CPT treat cells reacted with DAPI and TO-FH or with DAPI and TO-PRO 1. TO-FH bound the DNA of CPT treated (but not normal) Jurkat cells by FACS or confocal microscopy.

Compounds that fluoresce when intercalating with DNA, and do not cross cell membranes, serve as vital fluorochromes, differentiating membrane compromised necrotic cells from healthy cells. To see if TO-FH could be used in this fashion, we first employed a classic system for cell death studies, where Jurkat cells, a T cell lymphoma line, were induced into necrosis with camptothecin (CPT). Cells were then stained with Annexin V-Cy5.5 (Anx-Cy) and TO-FH, or Anx-Cy and TO-PRO 1, see Figure 5a−c. Control cells (−CPT, Figure 5a) failed to bind TO-FH or Anx-Cy except for a small population of necrotic cells. CPT increased the fraction of necrotic cells that bound both Anx-Cy and TO-FH (Figure 5b) or Anx-Cy and TO-PRO 1 (Figure 5c). Confocal microscopy (Figure 5d) indicated TO-FH and DAPI, a stain for DNA, were colocalized. Therefore, TO-FH behaved like a vital fluorochrome, failing to bind to or enter healthy cells while binding the DNA of necrotic cells. TO-PRO 1 produced a higher fluorescence than TO-FH per cell but the fractions of cells labeled TO-PRO 1 and TO-FH were similar, a situation analyzed quantitatively with the oxaliplatin/5-FU treated HT-29 cells used for a tumor model (Figure 6).

We next examined the interaction of TO-FH with HT-29 cells, a human adenocarcinoma cell line, using both cultured cells and an HT-29 xenograft. With permeabilization by 0.5% Tween 20 in PBS as a method of inducing necrosis, the binding of TO-FH, and two reference vital fluorochromes (TO-PRO 1 and Sytox

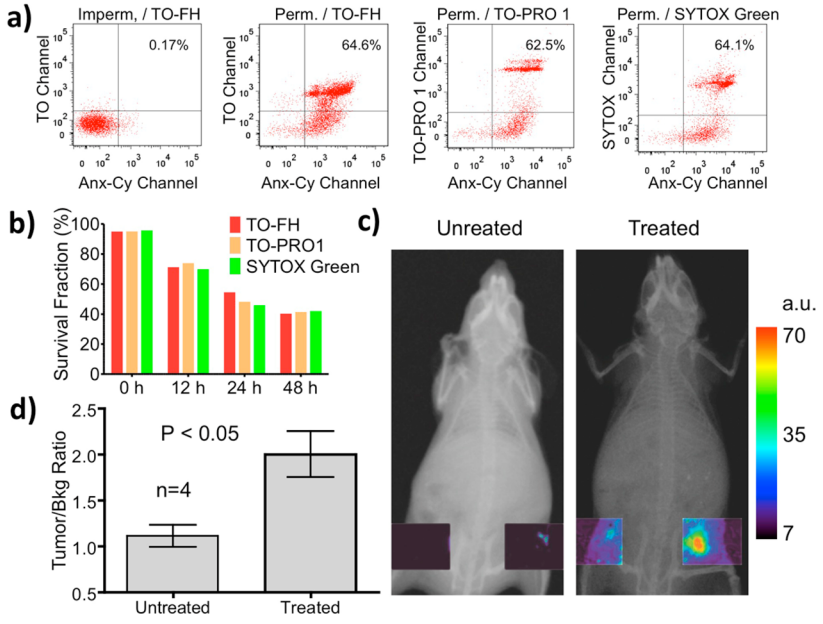

Figure 6. Interaction of TO-FH with HT-29 cells after permeabilization or after exposure to 5-FU/oxaliplatin treatment to induce cell death. (a) Normal or permeabilized cells were reacted with Anx-Cy and TO-FH or TO-PRO 1 or Sytox Green. (b) Cells were treated with 5-FU/oxaliplatin and exposed to Anx-Cy plus the indicated fluorochrome. Data are plotted as the survival fraction *versus* time of expose. Survival fraction is the percent of cells failing to bind both Anx-Cy and a second fluorochrome, *i.e.*, the lower left-hand quadrant of the scatter plot. With an increasing duration of treatment, the survival fraction falls. Survival fraction falls similarly with Anx-Cy and any of the three vital fluorochromes, TO-FH, TO-PRO 1, Sytox Green. (c) Tumor surface fluorescence after TO-FH injection with untreated and treated (5-FU/oxaliplatin) HT-29 xenografts. (d) Tumor fluorescence, measured as tumor/bkg fluorescence ($p < 0.05$), $n = 4$.

Green) were compared (Figure 6a). Only 0.17% of untreated, control HT-29 cells were TO-FH and Anx-Cy positive (*i.e.*, were necrotic cells, upper right quadrant), while permeabilization yielded between 62% and 65% necrotic cells for all three fluorochromes. Using treatment with oxaliplatin and 5-FU as a method of producing necrosis, the binding of all three fluorochromes was plotted as the survival fraction *versus* time of exposure as shown Figure 6b. The survival fraction is the percent of cells that fail to bind both Anx-Cy and a vital fluorochrome, *i.e.*, the lower left-hand quadrant of a dual-wavelength dot plot. The kinetics of cell death, as the decrease in survival fraction, was independent of the vital fluorochrome. (For example, $p > 0.05$, TO-FH *versus* Sytox Green for all time points).

We previously demonstrated that a low molecular weight gadolinium chelate of TO-PRO 1 bound the DNA of camptothecin (CPT) treated Jurkat cells,[25] and the DNA of cardomyocytes induced into necrosis by sustained vessel occlusion.[26] To determine whether the far larger TO-FH could be used to image the DNA of necrotic HT-29 cells, an HT-29 tumor was treated with 5-FU and oxaliplatin, followed by an IV injection of TO-FH. Experiments indicated that (i) both the fluorescence and relaxation enhancing properties of TO-FH were stable in mouse serum (see Supporting Information, Figure S2) and (ii) that the blood half-lives of the parent NP (FH) and TO-FH were 39.1 and 47.1 min, respectively, in normal mice (see Supporting Information Figure S3). *In vivo* images experiments were then conducted.

Surface fluorescence images of the tumors of treated and untreated animals 4 h, or approximately 5 blood half-lives, after injection were obtained as shown in Figure 6c. With this time point, TO-FH had cleared from the blood but had not been degraded and incorporated into hemoglobin. With oxaliplatin/5-FU treatment, tumor fluorescence was approximately twice that of untreated controls, with results significant at $p < 0.05$. A small focal signal intensity of untreated tumor reflects some tumor necrosis prior to the treatment with chemotherapeutic agents. Tumor fluorescence is shown because of gut fluorescence from dietary contents.

MR images of a treated (5-FU and oxaliplatin) HT-29 tumor are shown in Figure 7. In the preinjection image tumor signal intensity is relatively uniform (Figure 7a), with few areas of high signal intensity (blue) or low signal intensity (red) shown as colorized images of signal intensity superimposed on Figure 7a (7b). In the postinjection MR image (Figure 7c), areas of high signal intensity (blue arrows) and low signal (red arrows) are seen. Areas of high (blue) and low (red) signal intensity are shown in a colorized image of extreme signal intensities shown in Figure 7d.

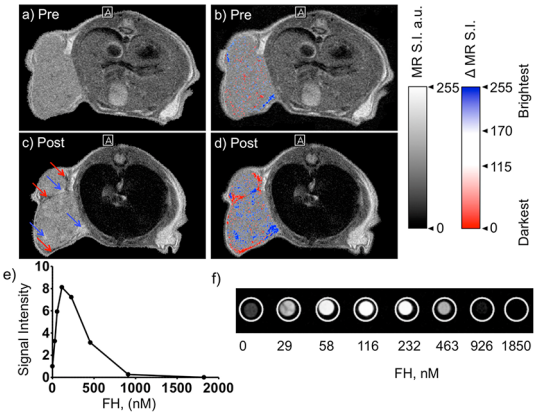

Figure 7. MR imaging of TO-FH uptake by the HT-29 tumor treated with oxaliplatin and 5-FU. (a) Pre-TO-FH image and (b) image from panel a with areas of highest signal intensity (brightest, blue) and lowest signal intensity (darkest, red) shown. Tumor is relatively uniform in signal intensity by MR signal intensity (a), with few areas high or low signal intensity shown by colorization (b). (c) Postinjection MR image. Regions of brightening (blue arrows) and darkening (red arrows) are seen. (d) Image from panel c with areas of highest signal intensity (brightest, blue) and lowest signal intensity (darkest, red) shown. (e) Signal intensity of FH solutions at varying concentrations of FH, in nM FH crystal, are shown from images (f). Using a T_1 weighted pulse sequence, TO-FH can brighten or darken MR images, either of a tumor (d) or phantoms (e, f).

To demonstrate the concentration-dependent brightening and darkening effects of TO-FH at the pulse sequence employed, phantoms with different iron concentrations were prepared and imaged with the pulse sequence used in Figures 7a–d. As shown in Figure 7e, low concentrations of TO-FH produced brightening, while high concentrations produced darkening, with signal intensities from Figure 7e as function of concentration plotted in Figure 7f. NP agents like FH or TO-FH, which have high r_1 as well as high r_2 values,[12,17] modest values of r_2/r_1, are brightening agents at low concentrations and darkening agents at high concentrations with T_1 weighted pulse sequences (see refs 27–29).

DISCUSSION

Fluorochrome-functionalized NPs are nanomaterials that employ DNA binding fluorochromes as the basis of their DNA recognition. Fluorochrome-functionalized NPs were synthesized by attaching variable numbers of the DNA intercalating fluorochrome TO-PRO 1 to the Feraheme (FH) NP, to generate a panel of TO-FH NPs with *n* values between 3.6 and 20. Advantages of using FH include its nontoxicity, superparamagnetism, thermal stability, and well-defined and well-described chemical and physical properties.

All TO-FHs formed TO-FH/DNA microaggregates at far lower EC50 values than were obtained with fluorescence (Table 2), reflecting multivalent interactions as shown in Figure 3d. At the EC50 values derived

from measurements of TO-FH/DNA microaggregate formation (T_2 or size), fluorochrome concentrations (provided by TO-FH NPs) exceeded the concentrations of intercalating sites available on DNA to accept them by between 3 and 10-fold. Hence when microaggregates formed, many fluorochromes on TO-FH were not involved with DNA binding and were not fluorescing (see Supporting Information, Table S2 for these calculations).

Theoretically, there is an enormous potential free energy gain from multivalent interactions as the polymeric calf-thymus DNA reacts with highly multivalent TO-FH. The MW of the calf thymus DNA is 8 400 000 Da,[30] and with a molecular weight of 1320 Da for a TO-PRO 1 intercalating binding site, there are 6400 sites for fluorochrome interaction on a molecule of DNA. (The molecular weight of a fluorochrome intercalation site is taken as a pair of base pairs, with a base pair weight of 660 Da.)[15,31] In a seminal paper on polyvalent interactions, Mammen *et al*. proposed that polyvalent interactions have affinities equal to $(K)^n$ (eq 5), where K is monomeric affinity constant and n is the number of independent, polyvalent binding sites.[32] However, the strong stacking interactions between TO-PRO 1s on the TO-FH surface (Figure 2c) are an energetic barrier that must be overcome for the intercalation reaction between TO-FH and DNA to occur, and this stacking complicates an understanding of the energetics of NP/DNA microaggregate formation.

This is first demonstration, to our knowledge, that a highly multivalent, nanoparticle like TO-FH can react with the DNA of necrotic cells, both in culture and with a tumor undergoing chemotherapy. TO-FH recognized the DNA of two cell lines (Jurkat and HT-29) after they underwent three necrosis-inducing treatments (CPT, permeabilization, 5-FU/oxaliplatin), while binding to normal vital cells was not detectable (Figures 5, 6). With CPT-treated Jurkat cells and confocal microscopy, TO-FH and DAPI colocalized, consistent with TO-FH binding to the DNA of cells induced into necrosis by CPT (Figure 5). With a necrosis induced by permeabilization or by treatment with 5-FU/oxaliplatin, TO-FH bound to the same populations of HT-29 cells as a commonly used vital fluorochrome Sytox Green (Figure 5). Using tumor surface fluorescence (Figure 6) and MR imaging (Figure 7), TO-FH accumulated in an HT-29 xenograft after 5-FU and oxaliplatin treatment.

The ability to bind the DNA of necrotic cells suggests the presence of pores in the plasma membrane large enough to allow the TO-FH NP to enter and bind DNA while sufficient plasma membrane integrity is maintained to confine target DNA. Some size-dependent delivery barriers to the larger TO-FH are present in necrotic cells, which were more fluorescent when reacted with the smaller TO-PRO 1 than the larger TO-FH. Consistent with this is the fact that the EC50s and maximum fluorescence of TO-FH and TO-PRO 1, when binding DNA *in vitro* are similar (Table 2).

Fluorochrome-functionalized NPs are a class of nanomaterials which, based on their recognition of DNA in biological systems, can serve as vital fluorochromes. TO-FH recognized the DNA of necrotic cultured cells or the DNA of tumor cells induced into necrosis by 5-FU/oxaliplatin. TO-FH bound to two cell lines (Jurkat and HT-29) after they underwent three necrosis-inducing treatments (CPT, permeabilization, 5-FU/oxaliplatin), while binding to normal vital cells was not detectable. With CPT-treated Jurkat cells and confocal microscopy, TO-FH and DAPI colocalized, consistent with TO-FH binding to the DNA of cells induced into necrosis by CPT. With a necrosis induced by permeabilization or by treatment with 5-FU/oxaliplatin, TO-FH bound to the same populations of HT-29 cells as a commonly used vital fluorochrome Sytox Green. Using tumor surface fluorescence or MRI, TO-FH accumulated in an HT-29 xenograft after 5-FU and oxaliplatin treatment (Figure 7).

However fluorochrome-functionalized NPs have a series of properties that make them far different from vital fluorochromes. First, fluorochrome-functionalized NPs are far larger than DNA binding fluorochromes. TO-FHs with different numbers of fluorochromes attached had diameters of 20−50 nm (Table 1, Figure 4), corresponding to proteins with molecular weights in excess of 750 kDa, while vital fluorochromes have molecular weights of less than about 1000 Da. Second, when injected, TO-FH had a blood half-life similar to the parent Feraheme NP, rather than the far more rapid clearance seen with low molecular weight materials. The blood half-life for TO-FH of 47.1 min in mice is relatively long for this rapidly metabolizing species, and comparable to the clearance of long circulating, high molecular weight dextrans.[33−35] Third, fluorochrome-functionalized NPs have superparamagnetic cores that allowed their reaction with DNA to be determined by relaxometry (or potentially by MRI). Finally, the conjugation of fluorochromes to NP surfaces provides a means of synthesizing DNA binding materials with valencies far above the divalency obtained with fluorochromes like TO-TO. High valency fluorochrome-functionalized NPs exhibit strong multivalent effects when binding DNA.

CONCLUSION

Multimodal and multivalent fluorochrome-functionalized NPs (TO-FH) are synthesized by attaching varying numbers of the TO-PRO 1 fluorochrome per NP to an aminated version of the Feraheme (FH) nanoparticle. Fluorochrome-functionalized NPs like

the TO-FH NP described here are a new class of DNA binding nanomaterials, one that binds DNA both *in vitro* and *in vivo*, and one with distinctive and useful properties in biomedical research.

MATERIALS AND METHODS

Materials. Feraheme (FH) was from AMAG Pharmaceuticals (Lexington, MA) and is their trademark. PD-10 columns were from GE Healthcare. Amicon centrifugal ultrafiltration units (50 kDa) were from Millipore. Ethylenediamine and EDC (1-ethyl-3-(3-dimethylaminopropyl) carbodiimide) were purchased from Pierce. Calf thymus DNA was from Sigma-Aldrich. Dialysis tubing (10 kDa) was from Spectrum Laboratories. Hydrodynamic size and zeta potential was measured with a Nano-ZS Zetasizer (Malvern, Marlboro, MA). Relaxation times were measured with a 20 MHz MiniSpec (Bruker Systems, Billerica, MA). Fluorescence of fluorochromes upon binding to DNA was calculated with a Glomax Multi Detection System (Promega, Madison, WI).

Synthesis of Fluorochrome-Functionalized NPs. Feraheme was aminated by reaction with ethylenediamine. An amount of 2 mL of FH (30 mg Fe/mL) was transferred to 0.1 M MES buffer, pH 5.5 using a PD-10. Ethylenediamine was added to the buffer-exchanged FH to bring its final concentration to 1 M, and EDC was mixed with the FH buffer at a concentration of 2 mg/mL. The mixture was reacted for 1 h at room temperature. The amine-modified FH was purified by gel filtration using a PD-10 column, followed by dialysis against PBS.

To synthesize fluorochrome-functionalized NPs, TO-NHS was synthesized[22] and added to amine-FH (500 μg of Fe in 10 mL of PBS) and the mixture reacted for 1 h at room temperature. Amounts of TO-NHS were varied between 0.05 mg and 0.5 mg to vary the number of TOs per NP. Nanoparticles were concentrated, and excess NHS-TOs were removed (Amicon Ultra 50K). Final purification employed a Sephadex G-25 PD-10 column (Supporting Information, Figure S1).

Characterization of Fluorochrome-Functionalized NPs. Conjugated TO-PRO 1 was determined using an extinction coefficient of 63 000 mM^{-1} cm^{-1} at 501 nm,[28,36] while iron concentrations were determined spectrophotometrically (300 nm) using a FH standard. The number of TO-PRO 1 NPs was determined from TO-PRO 1 and iron concentrations, with the value of 5874 Fe atoms per NP supplied by the manufacturer. Zeta potentials were determined after exchange into 40 mM Tris-HCl, pH 8. All other measurements were in PBS.

Reaction of Fluorochrome-Functionalized NPs with DNA. The EC50 values of vital dyes and fluorochrome-functionalized NPs for calf thymus DNA was examined by fluorescence, relaxometry, and light scattering. Calf thymus DNA was completely dissolved in tris-acetate-EDTA (TAE) buffer (pH = 8) by gentle inversion overnight at 4 °C. The stock DNA solution (0.5 mg/mL) was serially diluted from 250 μg/mL with a ratio of 1:3 in a 96 well plate. For the fluorescence response, the diluted DNA solutions were incubated with 50 nM of fluorochrome equivalents, as the common benzothiazole ring, for 2 h at 37 °C, and fluorescence was measured with the Glomax-Multi Detection System. For the comparison of binding affinities by fluorescence with T_2, the diluted DNA solutions were incubated with 1 μg Fe of fluorochrome-functionalized NPs. T_2 relaxation times were determined on a 20 MHz MiniSpec at 40 °C (Bruker Systems, Billerica, MA). The hydrodynamic size of the TO-FH/DNA microaggregates were measured by dynamic light scattering (DLS) using a zetasizer (Malvern Instruments, Marlboro, MA). Sample preparation for the light scattering was same as for T_2.

AFM of TO-FH/DNA Complexes. Two sets of samples were prepared for AFM imaging. One was calf thymus DNA diluted to a concentration of 39.6 μg/mL in 0.04 M tris-acetate-EDTA buffer (TAE), pH = 8. The other was a TO-FH/DNA complex sample incubated with 1 μg Fe of fluorochrome-functionalized NPs in TAE buffer. In each case, a quantity of 30 μL was deposited on a freshly cleaved mica substrate (9.9 mm, PELCO Mica Discs). The samples were incubated for 5 min to allow the DNA, TO-FH nanoparticles, and the aggregation to adhere to the substrate. The samples were then flushed using a volume of 1 mL of purified water to rinse off the unbound samples. They were then dried in air for 24 h. AFM imaging was performed in intermittent contact mode (Agilent 5500, acoustic AC mode). The tip used was an AAC N9621 (Agilent Technologies) with a resonant frequency of 159 kHz and a spring constant of 48 N/m. The images were recorded at 1024 by 1024 pixels at rate of 0.2 lines per second. To generate a histogram of size of TO-FH/DNA microaggregates, microaggregates which were larger than 5 nm threshold height were selected in a 5 μm $\times$ 5 μm AFM image of TO-FH/DNA complex sample because of the 5 nm average diameter of the core of the FH nanoparticle. Size measurements were made by fixing two end positions of each selected microaggregates in both horizontal and vertical cross sections and the PicoView software (Agilent Technology, Chandler, AZ) calculated the average distance of the two positions as a diameter.

Reaction of TO-FH with Jurkat Cells or HT-29 Cells. The three chemotherapeutic agents, 5-fluorouracil (5-FU), oxaliplatin, and camptothecin were dissolved in PBS to obtain 1 mM stock solutions. Cell lines were cultured and plated to 2 $\times$ 10^5 cells/well in a 24-well plate. Cells were incubated for one day before the chemotherapeutic treatment. HT-29 cells were exposed to two agents at final concentrations of 250 μM of 5-FU and 150 μM of oxaliplatin for the indicated times and Jurkat T cells were incubated with camptothecin (5 μM) for 10 h. After treatment, TO-FH (4 μg of Fe) was incubated for 1 h at 37 °C to be taken into cells. Cells were washed with Dulbecco's phosphate buffered saline (DPBS) and then detached (200 μL of 0.05% Trypsin with 0.53 mM EDTA, 10 min @ 37″C), pelleted (1500 rpm, 5 min), and resuspended in 300 μL of DPBS with Ca^{2+}, Mg^{2+}, and 1% fetal calf serum. Cells were stained with 1 μL of annexin V-Cy5.5 and 10 nM of SYTOX Green for 15 min at room temperature. Alternatively, TO-PRO 1 (100 nM) replaced SYTOX Green. A 1 mL portion of DPBS was added, and cells were pelleted as before, resuspended in 300 μL of DPBS, and analyzed with a FACSCalibur flow cytometer. To confirm cellular uptake of TO-FH and its binding to DNA, cells were permeabilized with 0.5% Tween 20 in PBS for 20 min. The permeabilized cell were washed with DPBS and collected as before for the flow cytometry.

Imaging the Response to Chemotherapy in HT-29 Tumor Bearing Mouse with TO-FH. All experiments were approved by the institutional animal care committee and used nu/nu mice (Charles River Laboratories, Wilmington, MA). To image chemotherapy induced necrosis, mice were implanted with 1 $\times$ 10^6 HT-29 human colorectal cancer cells (ATCC, Manassas, VA). When the xenograft tumors grew to a volume greater than 50 mm^3, a baseline imaging evaluation was performed. The animals received TO-FH (n = 4) at 5 mg Fe/kg *via* tail vein injection; 6 h later, the animals were anesthetized using 2% isoflurane in 1 L/min O_2 and imaged using a surface reflectance fluorescence imaging system (In Vivo Pro; Carestream, Rochester, NY), with an excitation filter of 480 nm and an emission filter of 535 nm. Two days later, animals were treated with the conventional combination chemotherapeutic regiment of 5-fluorouracil (5-FU; institutional clinical pharmacy) and oxaliplatin (LC Laboratories, Woburn, MA). The dosing regimen was as follows: the animals received 5-FU i.p. at 80 mg/kg, followed by oxaliplatin i.p. at 10 mg/kg 4 h later, and a second dose of 5-FU i.p. at 80 mg/kg 4 h after that. Six hours after the final chemotherapy dose, the animals were again administered either TO-PRO 1 or TO-FH *via* tail vein injection and imaged 6 h later using identical imaging parameters. Fluorescence data were analyzed by drawing manual regions of interest (ROIs) around the tumors as well as the contralateral normal flanks to calculate mean fluorescence signal intensities. Tumor to background ratios was calculated by dividing the former by the latter.

MR images were acquired using a permanent magnet MRI system from Bruker (ICON, 1T field). T_1-weighted images were acquired with a rapid acquisition with relaxation enhancement (RARE) sequence with the following parameter: repetition time = 761.9 ms, echo time = 30.0 ms. FOV = 2.76/2.41 cm. After a pre-TO-FH image was obtained, animals were injected as above and imaged 6 h later. Phantoms for MR imaging were prepared by diluting TO-FH in PBS to the indicated concentration. T_1-weighted images were again obtained.

Conflict of Interest: The authors declare no competing financial interest.

Supporting Information Available: Purification method of TO-FH, analysis of sites for intercalation, blood half-life of FH and TO-FH, and dot plots of detection of necrotic cells. This material is available free of charge *via* the Internet at http://pubs.acs.org.

REFERENCES AND NOTES

1. Marko, M. A.; Chipperfield, R.; Birnboim, H. C. A Procedure for the Large-Scale Isolation of Highly Purified Plasmid DNA Using Alkaline Extraction and Binding to Glass Powder. *Anal. Biochem.* **1982**, *121*, 382–387.
2. Boom, R.; Sol, C. J.; Salimans, M. M.; Jansen, C. L.; Wertheim-van Dillen, P. M.; van der Noordaa, J. Rapid and Simple Method for Purification of Nucleic Acids. *J. Clin. Microbiol.* **1990**, *28*, 495–503.
3. Ito, T.; Smith, C. L.; Cantor, C. R.; Sequence-Specific, D. N. A. Purification by Triplex Affinity Capture. *Proc. Natl. Acad. Sci. U.S.A.* **1992**, *89*, 495–498.
4. Rosi, N. L.; Giljohann, D. A.; Thaxton, C. S.; Lytton-Jean, A. K.; Han, M. S.; Mirkin, C. A. Oligonucleotide-Modified Gold Nanoparticles for Intracellular Gene Regulation. *Science* **2006**, *312*, 1027–1030.
5. Josephson, L.; Perez, J. M.; Weissleder, R. W. Magnetic Nanosensors for the Detection of Oligonucleotide Sequences. *Angew.Chem. Int. Ed.* **2001**, *40*, 3204–3206.
6. Perez, J. M.; Josephson, L.; O'Loughlin, T.; Hogemann, D.; Weissleder, R. Magnetic Relaxation Switches Capable of Sensing Molecular Interactions. *Nat. Biotechnol.* **2002**, *20*, 816–820.
7. Prodhomme, S.; Demaret, J. P.; Vinogradov, S.; Asseline, U.; Morin-Allory, L.; Vigny, P. A Theoretical and Experimental Study of Two Thiazole Orange Derivatives with Single- and Double-Stranded Oligonucleotides, Polydeoxyribonucleotides and DNA. *J. Photochem. Photobiol. B.* **1999**, *53*, 60–69.
8. Glazer, A. N.; Rye, H. S. Stable Dye–DNA Intercalation Complexes as Reagents for High-Sensitivity Fluorescence Detection. *Nature* **1992**, *359*, 859–861.
9. Serbedzija, G. N.; Dickinson, M.; McMahon, A. P. Cell Death in the CNS of the WNT-1 Mutant Mouse. *J. Neurobiol.* **1996**, *31*, 275–282.
10. Gorokhova, E.; Mattsson, L.; Sundstrom, A. M. A Comparison of TO-PRO-1 Iodide and 5-CFDA-AM Staining Methods for Assessing Viability of Planktonic Algae with Epifluorescence Microscopy. *J. Microbiol. Methods* **2012**, *89*, 216–221.
11. Wlodkowic, D.; Telford, W.; Skommer, J.; Darzynkiewicz, Z. Apoptosis and Beyond: Cytometry in Studies of Programmed Cell Death. *Methods Cell Biol.* **2011**, *103*, 55–98.
12. Alcantara, D.; Guo, Y.; Yuan, H.; Goergen, C. J.; Chen, H. H.; Cho, H.; Sosnovik, D. E.; Josephson, L. Fluorochrome-Functionalized Magnetic Nanoparticles for High-Sensitivity Monitoring of the Polymerase Chain Reaction by Magnetic Resonance. *Angew. Chem., Int. Ed.* **2012**, *51*, 6904–6907.
13. Benson, S. C.; Zeng, Z.; Glazer, A. N. Fluorescence Energy-Transfer Cyanine Heterodimers with High Affinity for Double-stranded DNA. I. Synthesis and Spectroscopic Properties. *Anal. Biochem.* **1995**, *231*, 247–255.
14. Petersen, M.; Hamed, A. A.; Pedersen, E. B.; Jacobsen, J. P. Bis-intercalation of Homodimeric Thiazole Orange Dye Derivatives in DNA. *Bioconjugate Chem.* **1999**, *10*, 66–74.
15. Benvin, A. L.; Creeger, Y.; Fisher, G. W.; Ballou, B.; Waggoner, A. S.; Armitage, B. A. Fluorescent DNA Nanotags: Supramolecular Fluorescent Labels Based on Intercalating Dye Arrays Assembled on Nanostructured DNA Templates. *J. Am. Chem. Soc.* **2007**, *129*, 2025–2034.
16. Balakrishnan, V. S.; Rao, M.; Kausz, A. T.; Brenner, L.; Pereira, B. J.; Frigo, T. B.; Lewis, J. M. Physicochemical Properties of Ferumoxytol, a New Intravenous Iron Preparation. *Eur. J. Clin. Invest.* **2009**, *39*, 489–496.
17. Li, W.; Tutton, S.; Vu, A. T.; Pierchala, L.; Li, B. S.; Lewis, J. M.; Prasad, P. V.; Edelman, R. R. First-Pass Contrast-Enhanced Magnetic Resonance Angiography in Humans Using Ferumoxytol, a Novel Ultrasmall Superparamagnetic Iron Oxide (USPIO)-Based Blood Pool Agent. *J. Magn. Reson. Imaging* **2005**, *21*, 46–52.
18. Groman, E. V.; Paul, K. G.; Frigo, T. B.; Bengele, H.; Lewis, J. M. Heat Stable Colloidal Iron Oxides Coated with Reduced Carbohydrates and Carbohydrate Derivatives. US Patent 6,599,498 B1. 2003.
19. Chen, S.; Alcantara, D.; Josephson, L.; Magnetofluorescent, A. Nanoparticle for *ex-vivo* Cell Labeling by Covalently Linking the Drugs Protamine and Feraheme. *J. Nanosci. Nanotechnol.* **2011**, *11*, 3058–3064.
20. Armitage, B. A. Cyanine Dye–DNA Interactions: Intercalation, Groove Binding, and Aggregation. *Top. Curr. Chem.* **2005**, *253*, 55–76.
21. Mullen, D. G.; Banaszak Holl, M. M. Heterogeneous Ligand-Nanoparticle Distributions: A Major Obstacle to Scientific Understanding and Commercial Translation. *Acc. Chem. Res.* **2011**, *44*, 1135–1145.
22. Hakem, I. F.; Leech, A. M.; Johnson, J. D.; Donahue, S. J.; Walker, J. P.; Bockstaller, M. R. Understanding Ligand Distributions in Modified Particle and Particlelike Systems. *J. Am. Chem. Soc.* **2010**, *132*, 16593–16598.
23. Perez, J. M.; Josephson, L.; Weissleder, R. Use of Magnetic Nanoparticles as Nanosensors to Probe for Molecular Interactions. *ChemBioChem.* **2004**, *5*, 261–264.
24. Galande, A. K.; Hilderbrand, S. A.; Weissleder, R.; Tung, C. H. Enzyme-Targeted Fluorescent Imaging Probes on a Multiple Antigenic Peptide Core. *J. Med. Chem.* **2006**, *49*, 4715–4720.
25. Garanger, E.; Hilderbrand, S. A.; Blois, J. T.; Sosnovik, D. E.; Weissleder, R.; Josephson, L. A DNA-Binding Gd Chelate for the Detection of Cell Death by MRI. *Chem. Commun. (Camb)* **2009**, 4444–4446.
26. Huang, S.; Chen, H. H.; Yuan, H.; Dai, G.; Schuhle, D. T.; Mekkaoui, C.; Ngoy, S.; Liao, R.; Caravan, P.; Josephson, L.; *et al.* Molecular MRI of Acute Necrosis with a Novel DNA-Binding Gadolinium Chelate: Kinetics of Cell Death and Clearance in Infarcted Myocardium. *Circ. Cardiovasc. Imaging* **2011**, *4*, 729–737.
27. Rogers, J.; Lewis, J.; Josephson, L. Use of AMI-227 as an Oral MR Contrast Agent. *Magn. Reson. Imaging* **1994**, *12*, 631–639.
28. Chambon, C.; Clement, O.; Le Blanche, A.; Schouman-Claeys, E.; Frija, G. Superparamagnetic Iron Oxides as Positive MR Contrast Agents: *In vitro* and *in vivo* Evidence. *Magn. Reson. Imaging* **1993**, *11*, 509–519.
29. Lutz, A. M.; Weishaupt, D.; Persohn, E.; Goepfert, K.; Froehlich, J.; Sasse, B.; Gottschalk, J.; Marincek, B.; Kaim, A. H. Imaging of Macrophages in Soft-Tissue Infection in Rats: Relationship between Ultrasmall Superparamagnetic Iron Oxide Dose and MR Signal Characteristics. *Radiology* **2005**, *234*, 765–775.
30. Porsch, B.; Laga, R.; Horsky, J.; Konak, C.; Ulbrich, K. Molecular Weight and Polydispersity of Calf-Thymus DNA: Static Light-Scattering and Size-Exclusion Chromatography with Dual Detection. *Biomacromolecules* **2009**, *10*, 3148–3150.
31. Persil, O.; Hud, N. V. Harnessing DNA Intercalation. *Trends Biotechnol.* **2007**, *25*, 433–436.
32. Mammen, M.; Chio, S.-K.; Whitesides, G. M. Polyvalent Interactions in Biological Systems: Implications for Design and Use of Multivalent Ligands and Inhibitors. *Angew. Chem., Int. Ed.* **1998**, *37*, 2754–2794.
33. Dreher, M. R.; Liu, W.; Michelich, C. R.; Dewhirst, M. W.; Yuan, F.; Chilkoti, A. Tumor Vascular Permeability, Accumulation,

and Penetration of Macromolecular Drug Carriers. *J. Natl. Cancer Inst.* **2006**, *98*, 335–344.
34. Kaneo, Y.; Uemura, T.; Tanaka, T.; Kanoh, S. Polysaccharides as Drug Carriers: Biodisposition of Fluorescein-Labeled Dextrans in Mice. *Biol. Pharm. Bull.* **1997**, *20*, 181–187.
35. Mehvar, R.; Robinson, M. A.; Reynolds, J. M. Molecular Weight Dependent Tissue Accumulation of Dextrans: *In vivo* Studies in Rats. *J. Pharm. Sci.* **1994**, *83*, 1495–1459.
36. Pei, R.; Stojanovic, M. N. Study of Thiazole Orange in Aptamer-Based Dye-Displacement Assays. *Anal. Bioanal. Chem.* **2008**, *390*, 1093–1099.